

PROPERTIES OF CENTRAL CAUSTICS IN PLANETARY MICROLENSING

SUN-JU CHUNG¹, CHEONGHO HAN^{1,9}, BYEONG-GON PARK², DOEON KIM¹, SANGJUN KANG³, YOON-HYUN RYU⁴, KANG MIN KIM²,
YOUNG-BEOM JEON², DONG-WOOK LEE⁵, KYONGAE CHANG⁶, WOO-BAIK LEE⁷, AND YONG HEE KANG⁸*Draft version October 29, 2021*

ABSTRACT

To maximize the number of planet detections, current microlensing follow-up observations are focusing on high-magnification events which have a higher chance of being perturbed by central caustics. In this paper, we investigate the properties of central caustics and the perturbations induced by them. We derive analytic expressions of the location, size, and shape of the central caustic as a function of the star-planet separation, s , and the planet/star mass ratio, q , under the planetary perturbative approximation and compare the results with those based on numerical computations. While it has been known that the size of the planetary caustic is $\propto \sqrt{q}$, we find from this work that the dependence of the size of the central caustic on q is linear, i.e., $\propto q$, implying that the central caustic shrinks much more rapidly with the decrease of q compared to the planetary caustic. The central-caustic size depends also on the star-planet separation. If the size of the caustic is defined as the separation between the two cusps on the star-planet axis (horizontal width), we find that the dependence of the central-caustic size on the separation is $\propto (s + s^{-1})$. While the size of the central caustic depends both on s and q , its shape defined as the vertical/horizontal width ratio, \mathcal{R}_c , is solely dependent on the planetary separation and we derive an analytic relation between \mathcal{R}_c and s . Due to the smaller size of the central caustic combined with much more rapid decrease of its size with the decrease of q , the effect of finite source size on the perturbation induced by the central caustic is much more severe than the effect on the perturbation induced by the planetary caustic. As a result, we find that although giant planets with $q \gtrsim 10^{-3}$ can be detected from the planet search strategy of monitoring high-magnification events, detecting signals of Earth-mass planets with $q \sim 10^{-5}$ will be very difficult. Although the central caustics of a pair of planets with separations s and s^{-1} are identical up to the linear order, we find that the magnification patterns induced by the pair of the degenerate caustics of planets with $q \gtrsim 10^{-3}$ are different to the level of being noticed from observations with $\lesssim 2\%$ photometry. Considering that the majority of planets to be detected by the strategy of monitoring high-magnification events are giant planets, we predict that the $s \leftrightarrow s^{-1}$ degeneracy could be broken for a majority of planetary events from observations with good enough precision.

Subject headings: planetary systems – planets and satellites: general – gravitational lensing

1. INTRODUCTION

Various methods have been proposed to detect and characterize extrasolar planets, including radial velocity technique (Mayor & Queloz 1995; Marcy & Butler 1996), transit method (Struve 1952), direct imaging (Angel 1994; Stahl & Sandler 1995), pulsar timing analysis (Wolszczan & Frail 1992), and microlensing (Mao & Paczyński 1991; Gould & Loeb 1992). See also the review of Perryman (2000). The microlensing signal of a planetary companion to Galactic disk and bulge microlens stars is the short-duration perturbation to the smooth standard light curve of the primary-induced lensing event occurred on background star. Compared to other methods, the decay of the planetary lensing signal with the decrease

of the planet/star mass ratio is relatively slow, and thus the microlensing technique has an important advantage of being applicable to the detections of Earth-mass planets by using already existing instrument (Bennett & Rhie 1996). The microlensing method also has a unique applicability to the detections of free-floating planets (Bennett & Rhie 2002; Han et al. 2004; Han, et al. 2005). In addition, the method is not restricted to planets of nearby stars and can be extended even to nearby galaxies (Baltz & Gondolo 2001). Recently, two clear-cut microlensing detections of exoplanets were reported by Bond et al. (2004) and Udalski et al. (2005).

Due to the rare and incidental chance of lensing events combined with the short duration of planet signals, planetary lensing searches require a special observational setup, where survey observations issue alerts of ongoing events in the early stage of lensing magnification (Soszyński et al. 2001; Bond et al. 2001) and follow-up collaborations intensively monitor the alerted events (Bond et al. 2002; Park et al. 2004; Cassan et al. 2004). However, follow-up is generally done with small field-of-view instrument, and thus events are monitored sequentially. As a result, only a handful number of events can be followed at any given time, limiting the number of planet detections. To maximize the number of potential planet detections with a limited use of resources and time, Griest & Safizadeh (1998) proposed to focus on high-magnification events. They pointed out that high-magnification events have a dramatically higher chance of being perturbed by planets due to the existence of a ‘cen-

¹ Department of Physics, Institute for Basic Science Research, Chungbuk National University, Chongju 361-763, Korea

² Bohyunsan Optical Astronomy Observatory, Korea Astronomy and Space Science Institute, Youngcheon 770-820, Korea

³ School of Liberal Arts, Semyung University, Jechon 390-711, Korea

⁴ Department of Astronomy and Atmospheric Sciences, Kyungpook National University, Daegu 702-701, Korea

⁵ Astrophysical Research Center for the Structure and Evolution of the Cosmos (ARCSEC), Sejong University, Seoul 143-747, Korea

⁶ Department of Computer and Applied Physics, Chongju University, Chongju 360-764

⁷ Korea Astronomy and Space Science Institute, Taejeon, Korea 305-348

⁸ Department of Earth Science Education, Kyungpook National University, Daegu 702-701, Korea

⁹ corresponding author; cheongho@astroph.chungbuk.ac.kr

tral' caustic (see § 2 for more detail). By adopting this proposal, current follow-up experiments are giving high priority to these events (Albrow et al. 2001; Rattenbury 2002; Bond et al. 2002; Abe et al. 2004; Jiang et al. 2004). However, little has been studied about the characteristics of central caustics and the perturbations induced by them (central perturbations).

In this paper, we investigate the properties of central caustics and the perturbations induced by them. The layout of the paper is as follows. In § 2, we describe basic physics of planetary lensing. In § 3, we analytically investigate how the location, size, and shape of the central caustic vary depending on the mass ratio, q , and separation, s , of planets under the planetary perturbative approximation and compare the results with those based on numerical computations. In § 4, we then systematically inspect the patterns of central perturbations by constructing maps of magnification excess for planets with various values of s and q . From the constructed maps, we also examine the effect of finite source size and investigate the possible types of planets detectable for given source stars with various sizes. We summarize the results and conclude in § 5.

2. BASICS OF PLANETARY LENSING

The lensing mapping from the lens plane to the source plane of N -point masses with no external shear or convergence is described by the lens equation of

$$\zeta = z - \sum_{j=1}^N \frac{m_j/M}{\bar{z} - \bar{z}_{L,j}}, \quad (1)$$

where $\zeta = \xi + i\eta$, $z_{L,j} = x_{L,j} + iy_{L,j}$, and $z = x + iy$ are the complex notations of the source, lens, and image positions, respectively, \bar{z} denotes the complex conjugate of z , m_j are the masses of the individual lens components, and $M = \sum_j m_j$ is the total mass of the lens system (Witt 1990). Here all angles are normalized to the Einstein ring radius θ_E of the total mass of the system, i.e.,

$$\theta_E = \frac{r_E}{D_L} = \left[\frac{4GM}{c^2} \left(\frac{1}{D_L} - \frac{1}{D_S} \right) \right]^{1/2}, \quad (2)$$

where D_L and D_S are the distances to the lens and source, respectively. For a single lens ($N = 1$), there exist two images with locations at $u_{l,\pm} = 0.5[u \pm (u^2 + 4)^{1/2}]$ and magnifications of $A_{\pm} = 0.5(A \pm 1)$, where $u \equiv |\zeta - z_L|$ is the separation between the lens and source. Then, the total magnification corresponds to the sum of the magnifications of the individual images and it is related to u by

$$A = A_+ + A_- = \frac{(u^2 + 2)}{u(u^2 + 4)^{1/2}}. \quad (3)$$

A planetary lensing is described by the formalism of a binary ($N = 2$) lens with a very low-mass companion. For a binary lens, there are three or five images and the number of images changes by two as the source crosses a caustic. The caustics are important features of binary lensing and they represent the set of source positions at which the magnification of a point source becomes infinite. The caustics of binary lensing form a single or multiple closed figures where each figure is composed of concave curves (fold caustics) that meet at cusps. For a planetary case, there exist two sets of disconnected caustics: one 'central caustic' located close to the host star and one or two 'planetary caustics' depending on whether

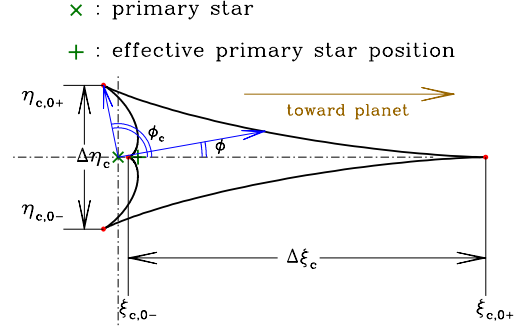


FIG. 1.— Geometry of a central caustic.

the planet lies outside or inside the Einstein ring. Since the central caustic lies close to the host star, the perturbation induced by the central caustic occurs close to the peak of lensing light curves of high-magnification events. For a star-planet system, it is known that the lensing behavior can be described by the perturbation approach due to the small planet/star mass ratio (Bozza 1999; Asada 2002; An 2005). In this case, the lensing equation is expressed as

$$\zeta = z - \frac{1}{\bar{z}} - \frac{q}{\bar{z} - \bar{z}_p}, \quad (4)$$

where the position of the star is chosen as the coordinate origin and z_p represents the location of the planet.

3. PROPERTIES OF CENTRAL CAUSTICS

Under the planetary perturbative approximation ($q \ll 1$ and $||z_p| - 1| \gg q$), the location of the central caustic can be expressed in an analytic form of

$$\zeta_c \simeq \frac{q}{2} e^{i\phi} \left[\frac{1}{(1 - z_p e^{-i\phi})^2} + \frac{1}{(1 - \bar{z}_p^{-1} e^{-i\phi})^2} - 1 \right] \quad (5)$$

(An 2005), where the polar coordinates are centered at the position of the primary star and ϕ represents the polar angle (see Figure 1). With the notation for the star-planet separation of $s = |z_p|$, the caustic position is expressed in an explicit form of

$$\xi_c \simeq \frac{s + s^{-1} + 2(\cos^3 \phi - 2 \cos \phi)}{(s + s^{-1} - 2 \cos \phi)^2} q, \quad (6)$$

$$\eta_c \simeq -\frac{2 \sin^3 \phi}{(s + s^{-1} - 2 \cos \phi)^2} q. \quad (7)$$

The central caustic has an elongated asteroid shape with four cusps, where two of them are located on the star-planet axis and the other two are located off the axis. Cusps of a central caustic occur when $d\zeta_c/d\phi = 0$ (i.e., when $\phi = 0$ and π for the on-axis cusps and when $\phi = \phi_c$ and $2\pi - \phi_c$ for the off-axis cusps), and thus their locations are found to be

$$\xi_{c,0\pm} \simeq \pm \frac{q}{(1 \pm s)(1 \pm s^{-1})}, \quad (8)$$

$$\eta_{c,0\pm} \simeq \pm \frac{2q |\sin^3 \phi_c|}{(s + s^{-1} - 2 \cos \phi_c)^2}, \quad (9)$$

FIG. 2.— Variations of the shape and size of the central caustic produced by planets with various separations from and mass ratios relative to the primary star. The left panels show the variations of the shape of the central caustic depending on the separation, while the right panels show the variation depending on the mass ratio. In all cases, coordinates are centered at the *effective* position of the host star and the planets are located on the left side. Note that the axis scales differ from one panel to another for better comparison of the caustic shapes.

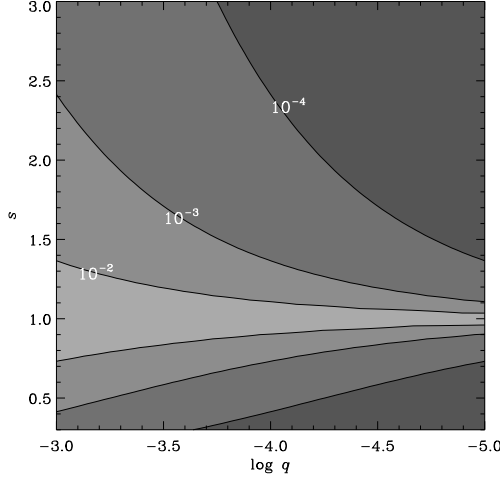


FIG. 3.— Size of the central caustic, as measured by the horizontal width, as a function of s and q .

where

$$\cos \phi_c = \frac{3}{4} \left(s + \frac{1}{s} \right) \left[1 - \sqrt{1 - \frac{32}{9} \left(s + \frac{1}{s} \right)^{-2}} \right]. \quad (10)$$

Then, the horizontal and vertical widths of the central caustic defined as the separations between the on- and off-axis cusps (see Figure 1) are respectively

$$\Delta \xi_c \simeq |\xi_{c,0+} - \xi_{c,0-}| = \frac{4q}{(s - s^{-1})^2}, \quad (11)$$

$$\Delta \eta_c \simeq |\eta_{c,0+} - \eta_{c,0-}| = \Delta \xi_c \frac{(s - s^{-1})^2 |\sin^3 \phi_c|}{(s + s^{-1} - 2 \cos \phi_c)^2}. \quad (12)$$

In Figure 2, we present central caustics produced by planets with various separations and mass ratios. From the figure and equations (5) – (12), we find the following characteristics of the central caustic.

1. The size of the central caustic depends on both the separation and mass ratio. The dependence of the central-caustic size on the mass ratio is linear, i.e., $\propto q$, as shown in equations (5) – (7) and demonstrated in the right panels of Figure 2. By comparison, the size of the planetary caustic is proportional to \sqrt{q} . This implies that the central caustic shrinks much more rapidly with the decrease of the planet mass compared to the planetary caustic. If the caustic size is defined as the horizontal width, the size depends on the star-planet separation by $\Delta \xi_c \propto (s + s^{-1})^{-2}$. Then, the caustic size becomes maximum when $s \sim 1$ and decreases with the increase of $|s - 1|$. In the limiting cases of a very wide-separation planet ($s \gg 1$) and a close-in planet ($s \ll 1$), the dependencies are respectively

$$\Delta \xi_c \propto \begin{cases} s^{-2} & \text{for } s \gg 1, \\ s^2 & \text{for } s \ll 1. \end{cases} \quad (13)$$

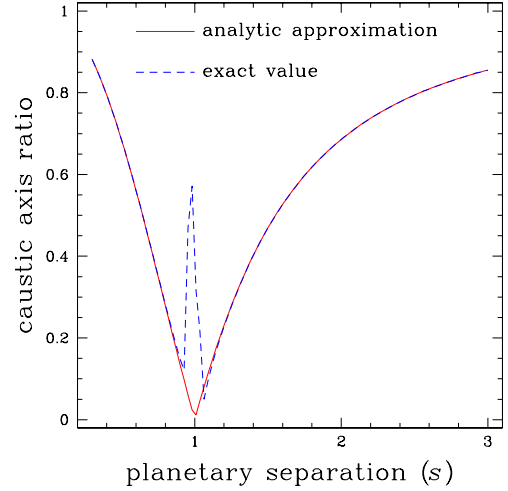


FIG. 4.— Dependence of the central-caustic shape, as measured by the ratio between horizontal and vertical widths, on the planet-star separation. The computations are based on planets with $q = 10^{-4}$.

In Figure 3, we present the size of the central caustic as a function of s and q .

2. For a given mass ratio, a pair of central caustics with separations s and s^{-1} are identical up to linear order. This can be seen from the pair of caustics with separations s and s^{-1} presented in Fig. 2. Analytically, this can also be proved from equations (5) – (7) where the inversion of $s \leftrightarrow s^{-1}$ result in the same expression.
3. Under the perturbative approximation, the shape of the central caustic is solely dependent on the planet separation. We quantify the caustic shape as the vertical/horizontal width ratio, $\mathcal{R}_c = \Delta \eta_c / \Delta \xi_c$, and present the variation of \mathcal{R}_c as a function of s in Figure 4. In the figure, we present two curves, where one is based on the perturbative approximation and the other is based on numerical computation. One finds that the width ratios based on the analytic and numerical computations match very well except the region around $s \sim 1$, where the perturbative approximation is not valid. We find that the difference in this region is caused by the merge of the planetary and central caustics.¹⁰ One also finds that the width ratio of the central caustic rapidly increases with the decrease of $|s - 1|$.

4. CENTRAL CAUSTIC PERTURBATIONS

Knowing now the characteristic of central caustics, we then investigate the pattern of planetary perturbations induced by central caustics. For this purpose, we construct maps of mag-

¹⁰ The planetary caustic produced by a planet with a separation s from its parent star is located at $\mathbf{x}_{pc} \sim s - 1/s$. Therefore, as $s \rightarrow 1$, $x_{pc} \rightarrow 0$, and thus the planetary caustic approaches the central caustic and eventually merge.

FIG. 5.— Contour maps of magnification excess as a function of source position (ξ, η) for planetary lens systems with various star-planet separations and planet/star mass ratios in the region around central caustics. Contours are drawn at the levels of $\epsilon = \pm 2\%$ (thin curves) and $\pm 5\%$ (thick curves) and greyscale is used to represent positive (bright) and negative (dark) deviation regions. All lengths are scaled by the Einstein ring radius corresponding to the total mass of the lens system. The coordinates are centered at the *effective* position of the host star. In all cases, planets are located on the left side. The maps are constructed for a *main-sequence* source star with a normalized radius of $\rho_* = 0.0018$, that corresponds to the case where the source with an absolute radius of $R_* = 1 R_\odot$ and located at $D_S = 8$ kpc is lensed by a lens with $m = 0.3 M_\odot$ and $D_L = 6$ kpc.

FIG. 6.— Contour maps of magnification excess for the same planetary lens systems as in Fig. 5, but for events associated with a *turn-off* source star with $\rho_* = 0.0054$.

TABLE 1
DETECTABILITY OF PLANETARY SIGNALS

source type	detectability		
	$q = 10^{-3}$	$q = 10^{-4}$	$q = 10^{-5}$
main-sequence ($\rho_* = 0.0018$)	O	O	X
turn-off ($\rho_* = 0.0054$)	O	\triangle	X
clump-giant ($\rho_* = 0.0234$)	O	X	X

NOTE. — The adopted source radius are $R_* = 1 R_\odot$, $3 R_\odot$, and $13 R_\odot$ for the main-sequence, turn-off, and clump giant stars, respectively. The normalized source radius $\rho_* = \theta_*/\theta_E$ of each source star is determined by choosing an Einstein ring radius of $\theta_E = 0.32$ mas that corresponds to the value of the most frequent Galactic bulge event with $m = 0.3 M_\odot$, $D_L = 6$ kpc, and $D_S = 8$ kpc. The individual symbols for the detectability represent possible ('O'), marginal (' \triangle '), and very difficult ('X'), respectively.

nification excess, which is defined as

$$\epsilon(\xi, \eta) = \frac{A - A_0}{A_0}, \quad (14)$$

where A is the exact magnification of the planetary lensing and A_0 is the single lensing magnification caused by the host star at its 'effective' position. Due to the additional deflection of light produced by the presence of the companion, it was known that the effective lensing position of a component of the binary lens system is shifted toward its companion (Di Stefano & Mao 1996; An & Han 2002). The amount of the shift of a lens component ' i ' toward the other component ' j ' is

$$\Delta x_{L,i \rightarrow j} \simeq \frac{m_j/m_i}{(s+s^{-1})/(\theta_{E,i}/\theta_E)} \frac{\theta_{E,i}}{\theta_E}, \quad (15)$$

where m_i and m_j are the masses of the individual lens components and $\theta_{E,i}$ is the Einstein ring radius corresponding to m_i (An & Han 2002). For a planetary lens case, the shift of the host star (with a notation ' \star ') toward the planet (with a notation ' p ') is expressed as

$$\Delta x_{L,\star \rightarrow p} \simeq \frac{q}{(s+s^{-1})}, \quad (16)$$

because $\theta_{E,\star} \sim \theta_E$ and $m_p/m_\star = q$.¹¹ Then, as either $|s-1| \rightarrow \infty$ (wide-separation planet) or $|s-1| \rightarrow 0$ (close-in planet), the shift is $\Delta x_{L,\star \rightarrow p} \rightarrow 0$, and thus the effective lensing position of the primary star approaches its original position.

¹¹ We note that the term ' s^{-1} ' in equations (15) and (16) was not included in the corresponding equations of Di Stefano & Mao (1996) and An & Han (2002), where they treated only wide-separation binaries. We introduce this term to keep the symmetry between the central caustics of planets with separations s and s^{-1} .

In Figure 5 – 7, we present the constructed magnification-excess maps for planets with various values of s and q . Planetary signal is important for planets with separations within the so called 'lensing zone' of $1/1.6 \lesssim s \lesssim 1.6$ (Gould & Loeb 1992), and thus we plot maps for planets located within this range. To see the effect of finite-source size, we construct three sets of maps with source stars of main-sequence (with a radius of $R_* = 1 R_\odot$), turn-off (with $R_* = 3 R_\odot$), and clump giant (with $R_* = 13 R_\odot$) stars and they are presented in Figure 5, 6, and 7, respectively. The magnification of a finite source with a surface brightness profile of $I(\zeta)$ is computed by the intensity-weighted magnification averaged over the source star surface, i.e.,

$$A_{fs}(\zeta) = \frac{\int_S I(\zeta') A(\zeta + \zeta') d\zeta'}{\int_S I(\zeta') d\zeta'}, \quad (17)$$

where A denotes the point-source magnification, ζ is the vector position of the center of the source, ζ' is the displacement vector of a point on the source star surface with respect to the source star's center, and the two-dimensional integral is over the source-star surface S . The effect of finite source size is smearing out the detailed structures of the planetary lensing signals. The finite-source effect is determined by the *normalized* source radius ρ_* , which represents the angular radius of a star, θ_* , in units of the Einstein ring radius, i.e. $\rho_* = \theta_*/\theta_E$. We thus set ρ_* of the individual stars by choosing an Einstein radius of $\theta_E = 0.32$ mas that corresponds to the value of the most frequent Galactic bulge event with $m = 0.3 M_\odot$, $D_L = 6$ kpc and $D_S = 8$ kpc. Then, the normalized source radius of a $R_* = 1 R_\odot$ star corresponds to $\rho_* = 0.0018$. For a source with uniform surface brightness, the computation can be reduced from a two-dimensional to a one-dimensional integral using the Generalized Stokes's theorem (Gould & Gaucherel 1997; Dominik 1998). To accelerate computations, we thus assume that the source stars have uniform surface brightness. However, we note that the effect of non-uniform surface brightness on the planetary lensing signal is not important. For a planetary system with a primary star of $m = 0.3 M_\odot$, the mass ratios of the Jupiter-, Saturn-, Neptune-, and Earth-mass planets correspond to $q \sim 3 \times 10^{-3}$, 10^{-3} , 10^{-4} , and 10^{-5} , respectively.

From the excess maps, we find the following properties of central perturbations.

1. First, we find that the effect of finite source size on central perturbations is much more severe than the effect on perturbations caused by planetary caustics. This is because the central caustic is not only much smaller but also shrinks much more rapidly with the decrease of q than the planetary caustic. As a result, we find that although giant planets with $q \gtrsim 10^{-3}$ can be detected from the planet search strategy of monitoring high-magnification events, detecting signals of Earth-mass planets with $q \sim 10^{-5}$ would be very difficult. It is

FIG. 7.— Contour maps of magnification excess for the same planetary lens systems as in Fig. 5, but for events associated with a *clump-giant* with $\rho_* = 0.0234$.

estimated that the lower mass limit of detectable planets will be that of a Neptune-mass planet with $q \sim 10^{-4}$, but detecting this mass-range planets will be possible only for events associated with source stars smaller than turn-off stars. In Table 1, we summarize the possible types of planets detectable from events involved with various types of source stars.

- Second, as expected by the close similarity between the pair of caustics with separations s and s^{-1} , the pattern of perturbations induced by these two caustics are similar each other. A good example is the pair of maps with $(s, q) = (1.2, 10^{-4})$ and $(1/1.2, 10^{-4})$ in Figure 5. However, we find that as the planet mass increases, the difference between the perturbation patterns of the pair of planets increases. We find that the difference is large enough to be noticed for planets with $q \gtrsim 10^{-3}$, c.f., the pair of maps of the planets with $(s, q) = (1.2, 10^{-3})$ and $(1/1.2, 10^{-3})$. Considering that the majority of planets to be detected by the strategy of monitoring high-magnification events are giant planets, we predict that the $s \leftrightarrow 1/s$ degeneracy could be broken for a majority of planetary events from observations with a $\lesssim 2\%$ photometric precision.

5. SUMMARY AND CONCLUSION

We investigated the properties of central caustics and the perturbations induced by them. Under the planetary perturbative approximation, we derived analytic expressions of the location, size, and shape of the central caustic as a function of the planet separation and mass ratio and compared the re-

sults with those based on numerical computations. While it has been known that the size of the planetary caustic is proportional to \sqrt{q} , we found from this work that the dependence of the central-caustic size on the mass ratio is linear. As a result, the central caustic shrinks much more rapidly with the decrease of the planet mass compared to the planetary caustic. Due to the large finite-source effect caused by the smaller size of the central caustic combined with much more rapid decrease of its size with the decrease of q , we predict that although giant planets with $q \gtrsim 10^{-3}$ can be detected from the planet search strategy of monitoring high-magnification events, detecting signals of Earth-mass planets with $q \sim 10^{-5}$ would be very difficult. Although the central caustics of a pair of planets with separations s and s^{-1} are identical up to the linear order, we found that the difference between the magnification patterns induced by the pair of degenerate caustics of planets with $q \gtrsim 10^{-3}$ can be noticed at the level of $\sim 2\%$. Because the majority of planets expected to be detected by the strategy of monitoring high-magnification events are giant planets, we predict that the $s \leftrightarrow s^{-1}$ degeneracy could be broken for a majority of planetary events from observations with good enough photometric precision.

We would like to thank J. H. An for making helpful comments. Work by C.H. was supported by the Astrophysical Research Center for the Structure and Evolution of the Cosmos (ARCSEC) of Korea Science and Engineering Foundation (KOSEF) through Science Research Program (SRC) program. B.-G.P. acknowledges the support from the grant of Korea Astronomy and Space Science Institute (KASI).

REFERENCES

- Abe, F., et al. 2004, *Science*, 305, 1264
 Albrow, M. D., et al. 2001, *ApJ*, 556, L113
 An, J. H., & Han, C. 2002, *ApJ*, 606, L155
 An, J. H. 2005, *MNRAS*, 356, 1409
 Angle, J. R. P. 1994, *Nature*, 368, 203
 Asada, H. 2002, *ApJ*, 573, 825
 Baltz, E. A., & Gondolo, P. 2001, *ApJ*, 559, 41
 Bennett, D. P., & Rhie, S. H. 1996, *ApJ*, 472, 660
 Bennett, D. P., & Rhie, S. H. 2002, *ApJ*, 574, 985
 Bond, I. A., et al. 2001, *MNRAS*, 327, 868
 Bond, I. A., et al. 2002, *MNRAS*, 333, 71
 Bond, I. A., et al. 2004, *ApJ*, 606, L155
 Bozza, V. 1999, *A&A*, 348, 311
 Cassan, A., et al. 2004, *A&A*, 419, L1
 Di Stefano, R., & Mao, S. 1996, *ApJ*, 457, 93
 Dominik, M. 1998, *A&A*, 333, L79
 Gould, A., & Loeb, A. 1992, *ApJ*, 396, 104
 Gould, A., & Gaucherel, C. 1997, *ApJ*, 477, 580
 Griest, K., & Safizadeh, N. 1998, *ApJ*, 500, 37
 Han, C., Chung, S.-J., Kim, D., Park, B.-G., Ryu, Y.-H., Kang, S., & Lee, D. W. 2004, *ApJ*, 604, 372
 Han, C., Gaudi, B. S., An, J. H., & Gould, A. 2005, *ApJ*, 618, 962
 Jiang, G., et al. 2004, *ApJ*, 617, 1307
 Mao, S., & Paczyński, B. 1991, *ApJ*, 374, L37
 Marcy, G. W., & Butler, R. P. 1996, *ApJ*, 464, L147
 Mayor, M., & Queloz, D. 1995, *Nature*, 378, 355
 Park, B.-G., et al. 2004, *ApJ*, 609, 166
 Perryman, M. A. C. Rep. Prog. Phys., 63, 1209
 Rattenbury, N. J., Bond, I. A., Skuljan, J., & Yock, P. C. M. 2002, *MNRAS*, 335, 159
 Soszyński, I., et al. 2001, *ApJ*, 552, 731
 Stahl, S. M., & Sandler, D. G. 1995, *ApJ*, 454, L153
 Struve, O. 1952, *Observatory*, 72, 199
 Udalski, A., et al. 2005, in preparation
 Witt, H. J. 1990, *A&A*, 236, 311
 Wolczen, A., & Frail, D. A. 1992, *Nature*, 355, 145

This figure "f2.jpg" is available in "jpg" format from:

<http://arxiv.org/ps/astro-ph/0505363v2>

This figure "f5.jpg" is available in "jpg" format from:

<http://arxiv.org/ps/astro-ph/0505363v2>

This figure "f6.jpg" is available in "jpg" format from:

<http://arxiv.org/ps/astro-ph/0505363v2>

This figure "f7.jpg" is available in "jpg" format from:

<http://arxiv.org/ps/astro-ph/0505363v2>